ADVANCED MATERIALS
www.advmat.de

www.MaterialsViews.com

Line Patterns from Cylinder-Forming Photocleavable Block Copolymers

*Weiyin Gu, Hui Zhao, Qingshuo Wei, E. Bryan Coughlin, Patrick Theato, and Thomas P. Russell**

Thin films of block copolymers (BCPs) self-assemble into arrays of nanoscopic microdomains with characteristic size scales of less than 100 nm and have attracted much interest from both the academic and industrial communities. The well-defined microdomains of BCP can be utilized for pattern transfer.[1,2] Consequently, there have been numerous studies that have focused on controlling the orientation and lateral ordering of the microdomains over large areas[3–5] and the incorporation of functional materials with a broad range of properties within the BCP microdomains, such as metals,[6,7] semiconductor quantum dots (QDs)[8] and functionalized nanoparticles.[9,10]

Recently, various studies have focused, not only on the orientation of the microdomains but also on the orientation of the direction of the lattice on the surface, i.e., a directed microdomain self-assembly of cylindrical microdomains in thin BCP films.[11–13] Polystyrene-block-poly(ethylene oxide) (PS-*b*-PEO), for example, has received considerable attention. Due to the unique chemical nature of the two blocks, these "amphiphile-like" polymers organize into well-defined nanostructured patterns, including lamellar, hexagonally-packed cylindrical, body-centered spherical, and bicontinuous gyroid microdomains. To achieve near-perfect lateral ordering requires the use of multiple external fields to fully direct the assembly, including thermal[14–16] and solvent annealing,[17–19] electro-magnetic fields,[20–22] and topographically and/or chemically patterned substrates.[23–25] Solvent annealing was first reported by Hashimoto[26] in the bulk and, later, by Libera[17] in thin films to induce long-range ordering of the BCP microdomain. Later, a similar effect was observed in PS-*b*-PEO thin films and a solvent gradient normal to the film surface was argued to give rise to the orientation of the microdomains, while the presence of the solvent imparted substantial mobility, enabling the "annealing" out of defects.[18] A significant number of studies have also appeared on the selective removal of one component of the BCP, e.g., by chemical etching,[27,28] UV degradation[29,30] and ozonolysis,[31] so that the nanoscopic BCP microdomain morphology could be used as a scaffold or template for the fabrication of nanostructured materials. Penelle and Russell[32] introduced the concept of using a reversible chemical cleavage of the junction point, converting a BCP into two homopolymers, which, if one of the blocks is ordered or far below its glass transition temperature, enable a simple removal of one of the blocks with a solvent that is a solvent for one block but not the other. Subsequently, Coughlin, Thayumanavan and Russell[33] designed a di-thio junction point that could easily be cleaved into the component homopolymers, enabling the use of a selective solvent to remove one component. More recently, several research groups have used the *o*-nitrobenzyl (ONB) ester group to constitute the junction point that can be used as an efficient, yet mild UV-cleavable linker between the two blocks and successfully developed this chemistry into a promising method to prepare nanoporous thin films.[34–38]

Cylindrical microdomains oriented normal to the surface of substrate that span the thickness of the films, can easily be used as a template for pattern transfer into an underlying magnetic material or as a scaffold into which magnetic materials can be deposited, with potential application as bit-patterned media for magnetic storage.[1,2] The promise of this technology has, in fact, placed the self-assembly of BCPs onto the Information Technology Roadmap (ITRC). If, however, the cylindrical microdomains are oriented parallel to the substrate, a fingerprint-type of pattern is observed, when the film is view from the top.[7,39] However, with the use of faceted surfaces, surface with a mild, highly oriented topographic pattern, then the cylindrical microdomains can be unidirectionally oriented, forming essentially a line pattern when viewed from the top which may open routes to applications ranging from nanolithographic masks,[40] multifinger devices (field effect transistor),[41] to photonic bandgap materials.[42,43] One distinct advantage of the cylindrical microdomain morphology over the lamellar microdomain morphology is that the cylindrical microdomains are more rigid and, as such, have a proclivity to maintain their orientation over very large distances.[12] In addition, if the minor component block, i.e., the cylindrical microdomains, can be selectively removed by ion beam methods, excellent pattern transfer can be achieved or well-defined trench patterns can be obtained that can be used for the fabrication of master templates for nanoscale imprint lithography (NIL). Key to this process is the complete removal of the minor component which is difficult by degradative processes or reconstruction processes,

W. Gu, Dr. Q. Wei,[+] Prof. E. B. Coughlin,
Prof. T. P. Russell
Department of Polymer Science and Engineering
120 Governors Drive
University of Massachusetts
Amherst, MA 01003, USA
E-mail: russell@mail.pse.umass.edu
Prof. P. Theato, H. Zhao
Institute for Technical and Macromolecular Chemistry
University of Hamburg
Bundesstr. 45, 20146 Hamburg, Germany
[+]Present Address: Nanosystem Research Institute (NRI), National Institute of Advanced Industrial Science and Technology (AIST), Tsukuba, Japan

DOI: 10.1002/adma.201301556

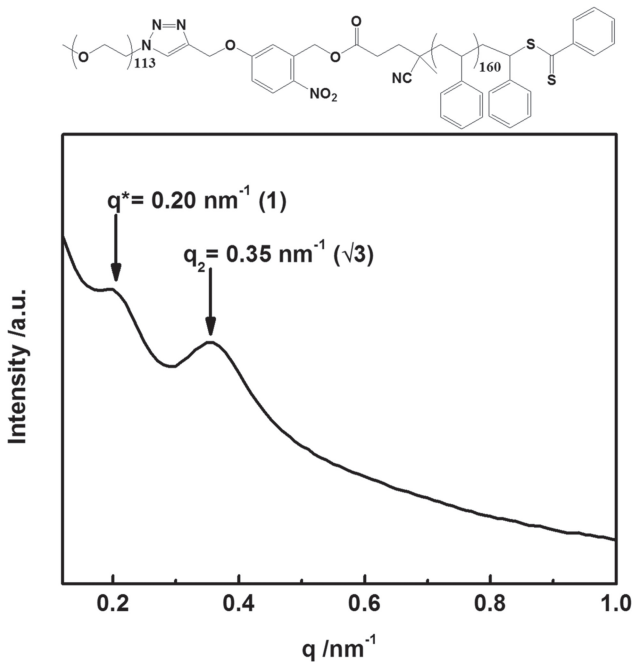

Figure 1. Chemical structure and SAXS of PS-*hν*-PEO (M_n = 21 kg mol^{-1}).

both of which are highly successful when the microdomains are oriented normal to the surface. However, by physically decoupling the two blocks into the constituent homopolymers using a simple chemical reaction, one is assured of a highly parallel process that will be driven to completion provided the components have sufficient mobility and can distance themselves from each other before recombining. Ross and coworkers[19,44] extensively studied the self-assembly of cylinder forming polystyrene-*block*-polydimethylsiloxane (PS-*b*-PDMS) copolymer, which is attractive for nanolithography because of its large χ and excellent etching contrast between PS and PDMS blocks. During an O_2 reactive-ion etching process, PS can be removed while PDMS can be converted to SiO_2. In their methods, pre-patterned substrates were often used in order to achieve good lateral order of PS-*b*-PDMS block copolymers. Here, we describe a simple photochemical reaction that can be used to cleave the junction point of a block copolymer and, by selective removal of the minor component, well-defined line patterns can be obtained without any surface guidance that are suitable for subsequent use a templates and scaffolds.

The photocleavable block copolymer PS-*hν*-PEO (M_n = 21 kg mol^{-1}) with a photocleavable *o*-nitrobenzyl (see inset in **Figure 1**) junction was synthesized by combining a RAFT polymerization of styrene followed by a PEO attachment using click chemistry, as described previously.[36] Small angle x-ray scattering (SAXS) was used to determine the bulk morphology of the BCP. As shown in Figure 1, the scattering showed a first order reflection at $q^* = 0.20$ nm^{-1} and a higher order peak at $q_2 = 0.35$ nm^{-1}. The relative scattering vectors (q_y) of the first two peaks were found to be 1:√3 indicating a hexagonal packing of the microdomains with repeat period, $L_o = 2\pi/q^*$, of 31.4 nm.

Procedures to deposit inorganic or metallic line structures prepared from self-assembled photocleavable block copolymer templates are outlined in **Scheme 1**. PS-*hν*-PEO BCP thin films were developed into well-ordered line patterns by solvent annealing (Scheme 1B) and then the minor PEO microdomains of the templates were removed by a mild UV irradiation at λ = 365 nm, which cleaved the BCP, followed by successive washing with a selective solvent of the minor block (Scheme 1C). The resultant templates were then used to fabricate: 1) silica line patterns using a simple spin coating with polydimethylsiloxane (PDMS) followed by an oxygen plasma exposure (Scheme 1D); and 2) metallic Au lines patterns by direct metal evaporation of Au onto the template, followed by a washing with toluene to lift-off the polymer template and overcoat of Au (Scheme 1E).

The surface morphology evolution with time of PS-*hν*-PEO thin films in tetrahydrofuran (THF) vapor, a neutral solvent for both blocks, was investigated by height and phase mode scanning force microscopy (SFM), as shown in **Figure 2**. PS-*hν*-PEO thin films were prepared by spin-coating a toluene solution (0.7 wt%) onto silicon substrates. The film thickness was

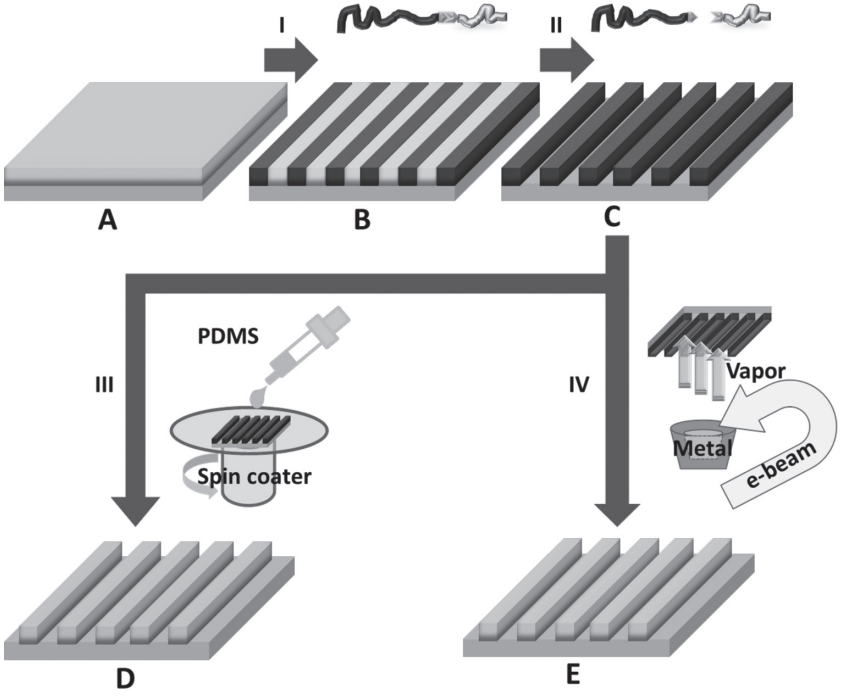

Scheme 1. Schematic illustration of silica and Au line patterns fabricated from photocleavable block copolymers. I) Solvent annealing of BCP films spin coated onto silicon substrates with a native oxide layer, II) UV exposure and followed by thoroughly solvent rinse to remove the minor block, III) filling the trenches with PDMS solution and subsequent conversion into silica line patterns by oxygen plasma treatment, IV) preparation of Au line patterns by electron-beam evaporation followed by a lift-off process.

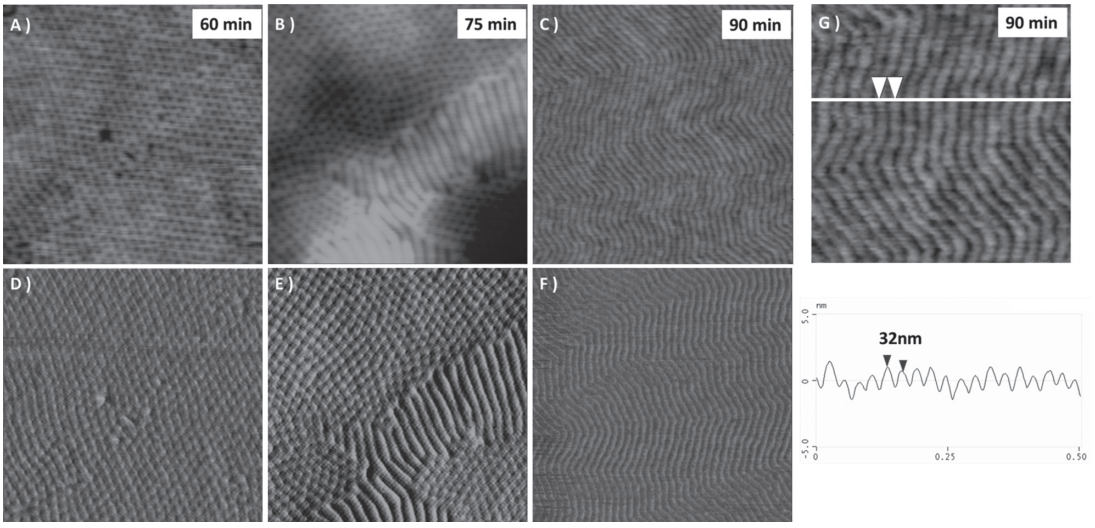

Figure 2. SFM height (A, B, C) and phase (D, E, F) images for PS-*hν*-PEO thin films (film thickness ~30 nm) after annealing in H_2O/THF atmosphere for 60 min (A, D), 75 min (B, E) and 90 min (C, F). As the solvent annealing time increases, cylindrical microdomains perpendicular to the silicon substrates are transformed into parallel orientation. G was a zoom-in image over a smaller area in terms of doing cross-sectional line cut analysis. Scale A-F: 1 μm × 1 μm; G: 500 nm × 500 nm.

kept ~1L_o, as confirmed by optical ellipsometry. Different orientations of the microdomains were obtained by varying the solvent annealing time. To prevent the thin films from dewetting, all films were pre-swollen in water for one hour.[12,23] The films were then annealed in THF vapor for 60 min. and well-ordered hexagonally arrays were observed, which resulted from PEO cylinders oriented normal to the surface of the film (Figure 2A and 2D). After 75 min. of annealing, the orientation of cylinders began to change from being normal to the surface to being parallel to the surface. A mixed morphology containing both orientations of the cylindrical microdomains was observed at intermediate annealing times (Figure 2B and 2E). After exposing the film to a solvent environment for 90 min. or longer, the orientation of the cylindrical microdomains was completely parallel to the substrate (Figure 2C and 2F). The mechanism for the change in the orientation of microdomains at different annealing time can be explained in terms of cylinder growth rate which varies as a function of position in the thin film.[45] When solvent annealing time increases, solvent concentration increases in the film while the growth rate of cylinders decreases moving into the film. Consequently, cylinders grow parallel to the substrate surface. The spacing between adjacent cylinders was determined from a line scan across the surface and found to be 32 nm (Figure 2G), which is in a good agreement with that determined by bulk SAXS measurements. These films with fully developed cylinders oriented parallel to the surface of the film were used to generate lines patterns (Supporting information, Figure S1).

With cylindrical microdomains oriented normal to the film surface, a reconstruction process can be used where the film is exposed to a good solvent for the minor component but a poor solvent for the matrix. This solubilizes the minor component, bringing it to the surface and, upon drying, leaves cylindrical pores in the film with the minor component, still chemically bonded to the major component, on the surface of the film.[6,7] Here, with the cylindrical microdomains oriented parallel to the surface, the same type of reconstruction will occur, even though the major component fully encases the cylindrical microdomain, i.e., there is a thin layer of the major component on the surface of the film. Here, after the film was immersed in ethanol, a good solvent for PEO and a nonsolvent for PS, reconstruction of the film occurred. **Figure 3**A and 3E show height and phase mode SFM images of the reconstructed films obtained from films annealed in solvent vapor for 90 min. and followed by reconstruction in ethanol for 30 min. Trenches can be observed, however, the boundaries between the microdomains were coarse, with large fluctuations and many defects, like discontinuities and bridging. This is understandable, due to the encasement of the minor component within the matrix PS and it is only the physical swelling of the minor component that causes a rupturing of the PS layer covering the PEO cylindrical microdomains. By comparison, imaging of photocleavable BCP thin films after UV irradiation and rinsing with methanol resulted in more distinctive patterns with cleaner and sharper interfaces, since the minor component is completely removed. Figure 3B and 3F show SFM height and phase images with high-quality trenches that were created after UV irradiation and thorough rinsing with methanol. Although UV cleavage of PEO was confirmed by various techniques in our previous report,[36] additional data can also be found in supporting information (Figure S2, gel permeation chromatography; Figure S3, x-ray photoelectron spectroscopy; Figure S4, attenuated total reflectance infrared spectroscopy; and Figure S5, transmission electron microscopy).

The well-ordered line patterns are good candidates for nanoscale templating. To demonstrate this, silica and Au line patterns were produced from these templates. Silica line patterns were prepared by spin-coating PDMS from a heptane solution onto the nanopatterned polymer film; oxidizing the PDMS with an oxygen plasma treatment (1 hour, 30 W, 0.2 bar

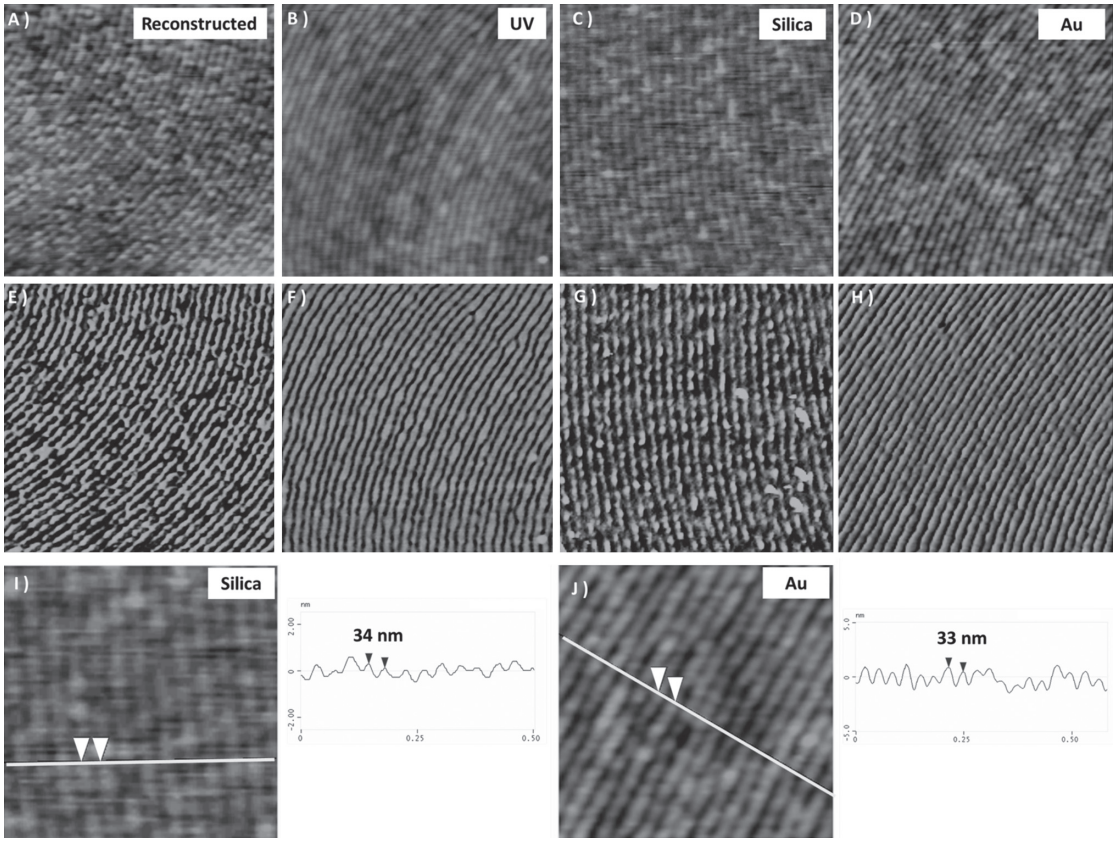

Figure 3. SFM height (A-D) and phase (E-H) images for PS-*hν*-PEO thin films with line patterns. The thin film was treated by 1) surface reconstruction in methanol (A, E); 2) UV cleavage and rinsing with methanol (B, F). The thin films treated by UV cleavage and rinsing with methanol were used to prepare silica (C, G) and Au line patterns (D, H). I and J were zoom-in images of C and D repectively in terms of doing cross-sectional line cut analysis. Scale A-H: 1 μm × 1 μm; I, J: 500 nm × 500 nm.

O_2); and then removing the PS homopolymer template with toluene. The resulting silica lines were imaged by SFM (Figure 3C and 3G). From the cross-sectional analysis (Figure 3I), a line pitch of ~34 nm was found, which is very close to that of the photocleavable BCP PS-*hν*-PEO template. The lateral order of silica lines also persisted from the photocleavable BCP PS-*hν*-PEO template.

Au line patterns were prepared by electron-beam deposition of Au onto the nanopatterned polymer film. The deposited metal layer was kept to ~10 nm, which is less than the total film thickness. A 2-nm thick titanium layer was deposited before Au (8 nm) to promote adhesion of the Au lines to the silicon substrates. To remove the polymer template, the Au-coated substrate was immersed in toluene, a good solvent for PS, for 30 min and rinsed with toluene thoroughly afterwards. Figure 3D and 3H are SFM height and phase images of well-ordered Au lines, respectively. A line pitch of ~33 nm was found, which is very close to that of the photocleavable BCP PS-*hν*-PEO template (Figure 3J, cross-sectional analysis). The Au line patterns were further characterized by scanning electron microscope (SEM), as shown in **Figure 4**. The width of Au lines was ~20 nm and the separation distance was ~35 nm, which is consistent with the dimension of line patterns after solvent annealing. Figure 4A and 4B show the top and tilted side view of the well-ordered Au metallic line patterns, respectively. The X-ray diffraction (XRD) pattern (Supporting information, Figure S6) of the Au lines showed a reflection with a Bragg spacing of 2.3 Å, which corresponds to the (111) plane of Au. From the full width at half maximum of the reflection, size of the Au crystals along the (111) direction was found to be

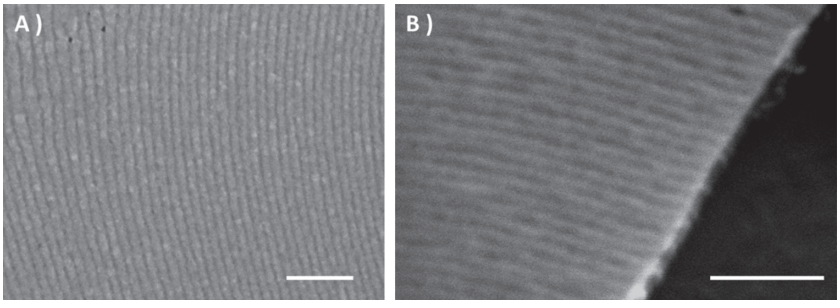

Figure 4. SEM images of A) top, B) tilted (~45°) views of Au line patterns prepared with PS-*hν*-PEO BCP. Scale bar: 200 nm.

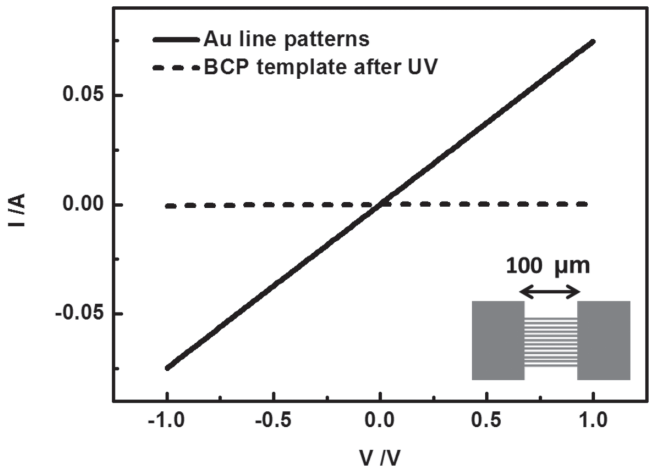

Figure 5. Current–voltage (*I–V*) curve obtained from gold nanowires and the BCP template.

13.6 nm using the Scherrer equation.[46] This is slightly smaller than the width of Au lines as measured by SEM.

To further investigate the properties of Au line patterns, current–voltage *(I–V)* curves were measured (**Figure 5**). For this, a 3-mm-long gold electrodes with a 100 μm gaps were prepared by electron-beam lithography on the silicon substrates (Figure 5, inset). For comparison, we also measured the I-V curves of silicon substrates with the BCP template before e-beam evaporation. Clearly no ohmic response for the polymer template before Au deposition was observed, while the I–V curves for the Au line patterns were linear. This linear response indicates that the lines constitute continuous, in-plane, metallic connections over an area of at least 3×10^5 μm^2. The resistivity of Au line patterns was calculated to be 3.2×10^{-6}, which differs significantly from that of bulk Au.[47] (Calculation method was shown in supporting information.) This difference is to be expected, given the widths of the lines and the possible existence of breaks or thin regions of the lines between the two electrodes. Nonetheless, generating continuous metallic nanolines by this facile BCP-templating process was clearly shown.

In summary, a versatile, simple method to prepare well-ordered line patterns from a photocleavable block copolymer PS-*hν*-PEO with an *o*-nitrobenzyl (ONB) junction was presented. Highly ordered PEO cylindrical microdomains oriented in the plane of the film were generated by solvent assisted directed self-assembly. By a photo-induced cleavage of the junction point to produce two homopolymers, removal of the minor component was straightforward to produce a trench-pattern that could be used as a template for pattern transfer or as a scaffold for the fabrication of oxide and metallic nanowires. This simple approach opens new routes for the fabrication of nanowires and device integration.

Experimental Section

Materials: Poly(styrene)-*block*-poly(ethylene oxide) PS-*b*-PEO ($M_{n,PS}$ = 15.7 kg mol^{-1}, $M_{n,PEO}$ = 5 kg mol^{-1}; PDI = 1.22) with an *o*-nitrobenzyl ester photocleavable junction (PS-*hν*-PEO) was synthesized by a combined RAFT polymerization and click chemistry approach. The synthetic methods and characterizations can be found in our previous report.[36]

Thin Film Preparation: The PS-*hν*-PEO BCPs thin films were prepared by spin-coating a toluene solution (0.7 wt%) onto silicon substrates and followed by solvent annealing in a H_2O/THF atmosphere for 2.5 h. The film thickness was controlled to be ~1 L_o. To cleave the PEO block, the thin films were kept in a quartz vacuum chamber under UV exposure at a wavelength of 365 nm and a dose of 5.6 J cm^{-2} (Blak-Ray Model B, UVL-56) for 12 hours. Finally the films were rinsed with methanol and dried by an air jet.

Silica Line Patterns from Photocleavable BCP Thin Film Templates: Polydimethylsiloxane (PDMS, Aldrich, Mw = 62 kg mol^{-1}) dissolved in heptane (0.1 wt%) was spin-coated onto the solvent annealed, UV-treated and rinsed PS-*hν*-PEO block copolymer films. The silicon substrate was further annealed on a hotplate at 60 °C for 1 hour to enhance the mobility of PDMS and draw the PDMS into the interstitial regions by capillary force. Finally, oxygen plasma treatment (1 hour, 30 W, 0.2 bar O_2) was performed to allow the transformation from PDMS into silica and removal of PS simultaneously.

Gold Line Patterns by E-Beam Evaporation: The CHA SE-600 electron beam evaporator with a 4 pocket hearth in the clean room was used to deposit the metal layer. The existence of Ti can increase the adhesion property of Au to the silicon substrates. Ti and Au were evaporated onto the silicon substrates subsequently at a pressure of 7×10^{-7} Torr to a nominal thickness of 2 nm and 8 nm at a rate of 0.01 nm/s, respectively, as measured by a quartz crystal microbalance.

Small Angle X-Ray Scattering (SAXS): SAXS was done using an in-house setup from Molecular Metrology Inc. It uses a 30 W microsource (Bede) with a 30 × 30 μm^2 spot size matched to a Maxflux optical system (Osmic) leading to a low-divergence beam of monochromatic CuK_α radiation (wavelength λ = 0.1542 nm). After passing beam-defining and guard pinholes, the beam of about 0.4 mm diameter enters the sample chamber. The SAXS intensity is collected by a two-dimensional gas-filled wire detector at a distance of about 1500 mm from the sample. A beamstop of 4 mm diameter in front of the detector has in its center a photodiode allowing monitoring the intensity of the direct beam. The sample was pressed between Kapton films and thermally treated at 150 °C for 24 hours before measurement.

Scanning Force Microscopy (SFM): SFM images were obtained in both the height and phase modes using Digital Instruments Dimension 3000 scanning force microscope with a Si probe (Veeco Instruments Inc., spring force constant 40 N m^{-1}) in tapping mode.

X-Ray Diffraction (XRD): The XRD pattern was recorded from an Au line patterns on the silicon substrates by using a PANalytical X'Pert diffractometer with CuK_α radiation (λ = 0.1542 nm) at a scanning rate of 0.05 degrees per second in 2θ ranging from 10° to 80°.

Scanning Electron Microscopy (SEM): Metal nanostructures on the silicon substrates were characterized by SEM (Magellan 400 made by FEI); imaging was typically performed with an electron energy of 5 keV.

Supporting Information

Additional SFM, GPC, XPS, ATR-IR, TEM and XRD data are provided. Supporting information is available from the Wiley Online Library or from the author.

Acknowledgements

This work was supported by the U.S. Department of Energy (DOE) under DOE DE-FG02-96E4612. We thank John Nicholson in the Nanofabrication Laboratory Facility (UMass, Amherst) for e-beam evaporation experiments and helpful discussion; we thank Louis Raboin and Alexander Ribbe in the W. M. Keck Electron Microscopy Facility (Umass Amherst) for the help about SEM measurements and helpful suggestions; we thank Jack Hirsch in the Surface Analysis Facility (Umass

Amherst) for the assistance of XPS experiments. Financial support from the German Science Foundation (DFG) under Grant TH 1104/4-1 and an International Collaboration in Chemistry award from the National Science Foundation (CHE 0924435) is gratefully acknowledged.

Received: April 8, 2013
Revised: May 18, 2013
Published online: July 19, 2013

[1] R. A. Segalman, *Mat. Sci. Eng. R.* **2005**, *48*, 191.
[2] J. N. L. Albert, T. H. Epps, *Mater. Today* **2010**, *13*, 24.
[3] T. L. Morkved, M. Lu, A. M. Urbas, E. E. Ehrichs, H. M. Jaeger, P. Mansky, T. P. Russell, *Science* **1996**, *273*, 931.
[4] I. Bita, J. K. W. Yang, Y. S. Jung, C. A. Ross, E. L. Thomas, K. K. Berggren, *Science* **2008**, *321*, 939.
[5] S. O. Kim, H. H. Solak, M. P. Stoykovich, N. J. Ferrier, J. J. de Pablo, P. F. Nealey, *Nature* **2003**, *424*, 411.
[6] S. Park, J. Y. Wang, B. Kim, T. P. Russell, *Nano. Lett.* **2008**, *8*, 1667.
[7] S. Park, B. Kim, A. Cirpan, T. P. Russell, *Small* **2009**, *5*, 1343.
[8] S. W. Yeh, T. L. Wu, K. H. Wei, *Nanotechnology* **2005**, *16*, 683.
[9] M. R. Bockstaller, Y. Lapetnikov, S. Margel, E. L. Thomas, *J. Am. Chem. Soc.* **2003**, *125*, 5276.
[10] Q. Zhang, T. Xu, D. Butterfield, M. J. Misner, D. Y. Ryu, T. Emrick, T. P. Russell, *Nano. Lett.* **2005**, *5*, 357.
[11] Y. S. Jung, C. A. Ross, *Nano. Lett.* **2007**, *7*, 2046.
[12] S. W. Hong, J. Huh, X. Gu, D. H. Lee, W. H. Jo, T. Xu, T. P. Russell, *PNAS* **2012**, *109*, 1402.
[13] H. S. Suh, H. Kang, C.-C. Liu, P. F. Nealey, K. Char, *Macromolecules* **2010**, *43*, 461.
[14] D. Y. Ryu, K. Shin, E. Drockenmuller, C. J. Hawker, T. P. Russell, *Science* **2005**, *308*, 236.
[15] P. Mansky, Y. Liu, E. Huang, T. P. Russell, C. Hawker, *Science* **1997**, *275*, 1458.
[16] C. A. Ross, Y. S. Jung, V. P. Chuang, J. K. W. Yang, I. Bita, E. L. Thomas, H. I. Smith, K. K. Berggren, G. J. Vancso, J. Y. Cheng, *J. Vac. Sci. Technol. B* **2008**, *26*, 2489.
[17] G. Kim, M. Libera, *Macromolecules* **1998**, *31*, 2569.
[18] S. H. Kim, M. J. Misner, T. Xu, M. Kimura, T. P. Russell, *Adv. Mater.* **2004**, *16*, 226.
[19] J. G. Son, J.-B. Chang, K. K. Berggren, C. A. Ross, *Nano. Lett.* **2011**, *11*, 5079.
[20] T. Xu, J. Stevens, J. A. Villa, J. T. Goldbach, K. W. Guarini, C. T. Black, C. J. Hawker, T. P. Russell, *Adv. Funct. Mater.* **2003**, *13*, 698.
[21] K. Schmidt, H. G. Schoberth, M. Ruppel, H. Zettl, H. Hänsel, T. M. Weiss, V. Urban, G. Krausch, A. Böker, *Nat. Mater.* **2007**, *7*, 142.
[22] P. W. Majewski, M. Gopinadhan, C. O. Osuji, *J. Polym. Sci. Pol. Phys.* **2012**, *50*, 2.
[23] S. Park, D. H. Lee, J. Xu, B. Kim, S. W. Hong, U. Jeong, T. Xu, T. P. Russell, *Science* **2009**, *323*, 1030.
[24] J. Xu, S. Park, S. Wang, T. P. Russell, B. M. Ocko, A. Checco, *Adv. Mater.* **2010**, *22*, 2268.
[25] S. Xiao, X. Yang, S. Park, D. Weller, T. P. Russell, *Adv. Mater.* **2009**, *21*, 2516.
[26] T. Hashimoto, M. Shibayama, H. Kawai, *Macromolecules* **1980**, *13*, 1237.
[27] J. M. Leiston-Belanger, T. P. Russell, E. Drockenmuller, C. J. Hawker, *Macromolecules* **2005**, *38*, 7676.
[28] L. Chen, W. A. Phillip, E. L. Cussler, M. A. Hillmyer, *J. Am. Chem. Soc* **2007**, *129*, 13786.
[29] P. Mansky, C. K. Harrison, P. M. Chaikin, R. A. Register, N. Yao, *Appl. Phys. Lett.* **1996**, *68*, 2586.
[30] J. Bang, S. H. Kim, E. Drockenmuller, M. J. Misner, T. P. Russell, C. J. Hawker, *J. Am. Chem. Soc.* **2006**, *128*, 7622.
[31] T. Thurn-Albrecht, J. Schotter, G. A. Kästle, N. Emley, T. Shibauchi, L. Krusin-Elbaum, K. parini, C. T. Black, M. T. Tuominen, T. P. Russell, *Science* **2000**, *290*, 2126.
[32] J. T. Goldbach, T. P. Russell, J. Penelle, *Macromolecules* **2002**, *35*, 4271.
[33] M. Zhang, L. Yang, S. Yurt, M. J. Misner, J.-T. Chen, E. B. Coughlin, D. Venkataraman, T. P. Russell, *Adv. Mater.* **2007**, *19*, 1571.
[34] H. Zhao, E. Sterner, E. B. Coughlin, P. Theato, *Macromolecules* **2012**, *45*, 1723.
[35] M. Kang, B. Moon, *Macromolecules* **2009**, *42*, 455.
[36] H. Zhao, W. Gu, E. Sterner, T. P. Russell, E. B. Coughlin, P. Theato, *Macromolecules* **2011**, *44*, 6433.
[37] J.-M. Schumers, J.-F. Gohy, C.-A. Fustin, *Polym. Chem.* **2010**, *1*, 161.
[38] C. G. Gamys, J.-M. Schumers, A. Vlad, C.-A. Fustin, J.-F. Gohy, *Soft Matter* **2012**, *8*, 4486.
[39] M. P. Stoykovich, P. F. Nealey, *Mater. Today* **2006**, *9*, 20.
[40] C. A. Ross, J. Y. Cheng, *MRS Bull.* **2008**, *33*, 838.
[41] S. M. Park, O. H. Park, J. Y. Cheng, C. T. Rettner, H. C. Kim, *Nanotechnology* **2008**, *19*, 455304.
[42] Y. Fink, D. J. Ripin, S. Fan, J. D. Joannopoulos, E. L. Thomas, *J. Lightwave Technol.* **1999**, *17*, 2039.
[43] Y. Kang, J. J. Walish, T. Gorishnyy, E. L. Thomas, *Nat. Mater.* **2007**, *6*, 957.
[44] J. K. W. Yang, Y. S. Jung, J.-B. Chang, R. A. Mickiewicz, A. Alexander-Katz, C. A. Ross, Karl K. Berggren, *Nat. Nanotechnol.* **2010**, *5*, 256.
[45] W. A. Phillip, M. A. Hillmyer, E. L. Cussler, *Macromolecules* **2010**, *43*, 7763.
[46] J. I. Langford, A. J. C. Wilson, *J. Appl. Cryst.* **1978**, *11*, 102.
[47] J. Chai, D. Wang; X. N. Fan, J. M. Buriak, *Nat. Nanotechnol.* **2007**, *2*, 500.